


# DC pulsed plasma magnetron sputtering of CdO/Cu/CdO multilayers thin films for self-cleaning and optoelectronic applications

Alzahra A. Abd El-Moula<sup>1</sup>, Mohamed Raaif<sup>2,3</sup>, Fayez El-Hossary<sup>2</sup>, and Mohamed Abo El-Kassem<sup>2,\*</sup> 

<sup>1</sup> Physics Department, collage of Science, Juof University, PO Box 2014, Sakaka, Saudi Arabia

<sup>2</sup> Physics Department, Faculty of Science, Sohag University, Sohag 82524, Egypt

<sup>3</sup> Physics Department, Faculty of Science and Arts, Al-Mandaq, Al-Baha University, 65755, Saudi Arabia

Received 30 October 2022 / Accepted 28 February 2023

**Abstract.** In this study, CdO/Cu/CdO multilayers thin films were organized on glass substrates with different Cu intermetallic layer thickness engaging DC plasma magnetron sputtering. The optoelectronic properties and structural characteristics of the multilayers at various Cu intermetallic layer thicknesses which were varied from 4 to 16 nm were explored. The calculated band gap was reduced from 2.66 eV to 2.48 eV as the Cu intermetallic layer thickness increased from 4 to 16 nm. The refractive index and coefficient of extinction of CdO/Cu/CdO multilayers increased with increasing the Cu intermetallic layer thickness. The resistivity is reduced from  $1.8 \times 10^{-2} \Omega \text{ cm}$  for CdO single layer to reach a value of  $2.7 \times 10^{-4} \Omega \text{ cm}$  for CdO/Cu (16 nm)/CdO multilayer. Further, the sheet resistance is decreased from 1000 to  $13.8 \Omega/\text{sq.}$  with the variation in Cu intermetallic layer thickness from 0 to 16 nm. CdO/Cu (4 nm)/CdO multilayer film recorded the best figure of merit ( $2.3 \times 10^{-4} \Omega^{-1}$ ). After sunlight illumination for the multilayers, the surface wettability was improved and the contact angle recorded lowest value of nearly  $24^\circ$  for CdO/Cu (8 nm)/CdO and CdO/Cu (12 nm)/CdO.

**Keywords:** Optical properties, CdO/Cu/CdO multilayers, Surface wettability.

## 1 Introduction

Furthermost transparent conducting oxides (TCOs) are binary or ternary compounds, enclosing one or two metallic elements. The resistivity of the TCO materials could be as low as  $10^{-3}$ – $10^{-4} \Omega \text{ cm}$  and the extinction coefficient in the optical visible range about 0.0001, in addition to their wide optical band gap that could be about 3 eV. Optimizing the optical transparency along with the electrical conductivity are frequently incredible in intrinsic stoichiometric oxides. In order to achieve this, they are constructed with a non-stoichiometric composition with suitable dopants or through bi/tri-layered structure with an appropriate intermetallic layer. In fact, thin films of ZnO,  $\text{In}_2\text{O}_3$ , and SnO were recognized as TCOs [1–3]. However, doping or tri-layer structure for these oxides resulted in enhancing the electrical conductivity without harshly reduced the optical transmission. From all the TCOs, indium tin oxide (ITO) is widely used for different applications such as hetero-junction silicon wafer solar cells [1] and transparent

electrodes [4]. On the other hand, cadmium oxide (CdO) is one of the TCOs materials [5, 6]. It has n-type semiconducting nature with good electrical resistivity of nearly  $10^{-2}$ – $10^{-4} \Omega \text{ cm}$  and has moderate transparency (<70%) in the visible and near infrared regions. Additionally, CdO has worthy stability for chemical and temperature reactions, good mechanical strength because of its cubic structure. However, cadmium oxide is considered as a toxic substance. The wettability of the materials plays a considerable role in solar cell technology. The self-cleaning surfaces may be employed as solar panel coatings because they help in the elimination of dirt and dust thereby enhancing their light transmittance and energy conversion efficiency. The surfaces' wettability can be commonly categorized into two types: (i) hydrophobic surfaces and (ii) hydrophilic surfaces [7–9]. In hydrophobic surfaces, the contact angle between the surface and water is equal to or greater than  $90^\circ$ . The drops of water roll on the surface and carry the dirt from the surface. In the case of hydrophilic surfaces, the contact angle between the surface

\* Corresponding author: [m.aboel-kassem@science.sohag.edu.eg](mailto:m.aboel-kassem@science.sohag.edu.eg)

and water is less than  $90^\circ$ . The drops of water spread on the surface and form a thin layer of water. After that, the dirt is washed away during the spreading process. In this work, CdO/Cu/CdO multilayer thin films were deposited on glass substrate by DC pulsed plasma magnetron sputtering. The effect of Cu intermetallic layer thickness on the optoelectronic properties of the multilayers was examined. Further, the effect of sunlight illumination on the surface wettability of the CdO/Cu/CdO multilayer films was explored.

## 2 Experimental procedures

### 2.1 Thin film preparation

DC pulsed magnetron sputtering system [10] was engaged to deposit multilayer films of CdO/Cu/CdO on glass substrates. A stainless steel chamber (30 cm diameter) was evacuated using turbo and rotary pumps to realize a base pressure of  $5 \times 10^{-6}$  mbar. Pure Ar as a sputtering gas and  $O_2$  as a reactive gas were mixed to deposit CdO layers from Cd target (purity: 99.99%, diameter: 2 inch and thickness: 3 mm) with partial pressures of  $4.5 \times 10^{-3}$  and  $0.5 \times 10^{-3}$  mbar for Ar and  $O_2$ , respectively. While pure Ar gas was employed to deposit the Cu intermetallic layer from Cu target (purity: 99.99%, diameter: 2 inch and thickness: 3 mm). The multilayer films were deposited continuously without opening the chamber. To eliminate the vacuum chamber and targets contaminations and consequently thin film contaminations, both Cd and Cu targets were cleaned by sputtering with pure argon for 10 min before depositing both Cu intermetallic and CdO layers. The total employed pressure for depositing CdO/Cu/CdO multilayer films was reserved at  $5 \times 10^{-3}$  mbar. The plasma processing power (DC-pulsed power supply model: Pinnacle Plus) was regulated at 50 and 20 W for depositing both CdO layers and Cu interlayers, respectively. The frequency (frequency of the square wave power supply) and reverse time (the time of signal off) were established at 150 KHz and 2  $\mu$ s, respectively. The space between the substrate and the target was held at 5 cm. CdO layers were deposited at a rate of roughly  $4.5 \text{ \AA}/\text{s}$  with thickness of nearly  $90 \pm 2 \text{ nm}$  for both bottom and top layers. The Cu interlayer was deposited at a rate of  $5 \text{ \AA}/\text{s}$  and the Cu metallic interlayer thickness was changed from 4 nm to 16 nm. It should be stated that the thickness monitor (Inficon SQM-160) was engaged for monitoring the deposition rate and multilayer film thickness.

### 2.2 Thin film characterization

The phase configurations of CdO/Cu/CdO multilayer films were inspected using a Bruker XRD D8 Advanced with Cu-K $\alpha$  radiation (1.542  $\text{\AA}$ ) in  $\Theta$ - $2\Theta$  with grazing incidence of  $2^\circ$  and step interval of  $0.02^\circ$ . The transmittance and reflectance at normal incidence were measured using a Jasco V-670 UV-Vis-NIR in the wavelength range of 200–2500 nm. The room temperature electrical resistance was recorded using the two-probe method. The resistivity ( $\rho$ ) was calculated from the equation  $\rho = \frac{RA}{L}$ , where  $R$  is the

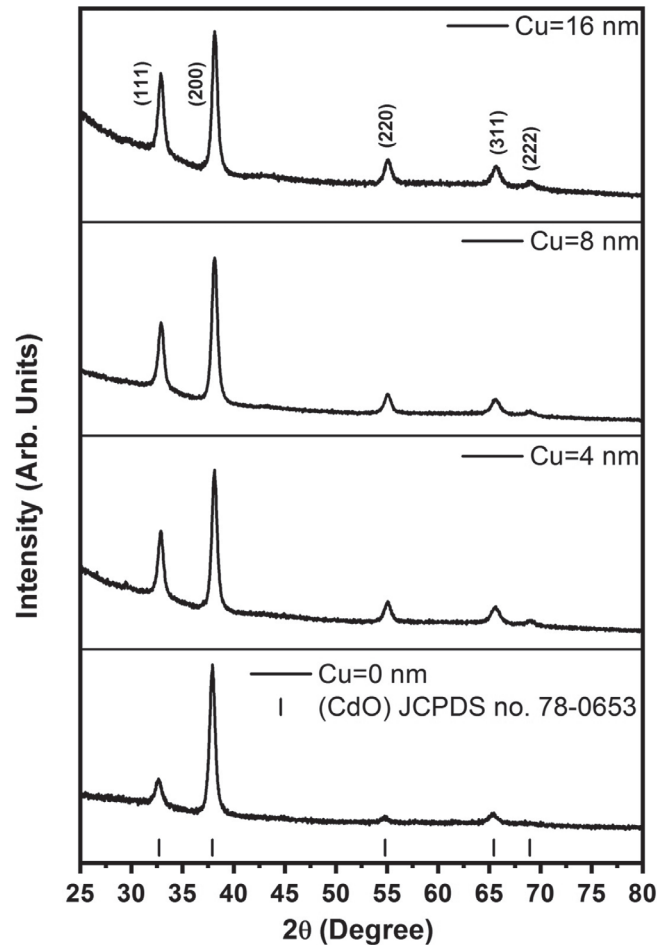


**Fig. 1.** XRD patterns of CdO/Cu/CdO multilayer films with different Cu metallic interlayer thickness.

resistance,  $A$  is the cross-sectional area ( $\text{cm}^2$ ), and  $L$  is the length (cm). Two silver paste electrodes with a separated distance of  $L = 0.2 \text{ cm}$  were placed on the surface of the multilayer films, and the sheet resistance ( $R_s$ ) was calculated by dividing the resistivity by the film thickness. Details about the two-probe method can be found elsewhere [11]. The surface wettability was assessed by determining the water contact angles between multilayers film surface and pure water before and after sunlight illumination for one-hour duration by a PHONIX-300 contact angle meter.

## 3 Results and discussion

### 3.1 Multilayers characterization

The XRD patterns of CdO/Cu/CdO multilayers thin films with different Cu intermetallic layer thickness are presented in Figure 1. One can witness from the figure that the CdO/Cu/CdO multilayer films are polycrystalline in nature. Broad and well-defined XRD peaks are observed for CdO/Cu/CdO multilayer thin films with different metallic Cu thickness corresponding to CdO phase at  $2\Theta = 32.83^\circ$ ,

**Table 1.** Different micro-structural parameters of CdO/Cu/CdO multilayer films with different Cu metallic interlayer thickness.

Cu thickness (nm)	Lattice parameter (a) Å	Crystallite size (nm)	Percentage of the positive angle shift (%)	Dislocation density $\delta \times 10^{15}$ (lines m <sup>-2</sup> )	Micro strain $\epsilon \times 10^{-3}$	Number of crystallites per unit area (10 <sup>16</sup> crystallites m <sup>-2</sup> )	Texture coefficient (200)
0	4.739	12.03	0	6.91	8.74	10.34	–
4	4.713	14.46	0.455	4.32	8.58	5.25	1.00142
8	4.715	15.22	0.396	4.78	8.4	6.22	1.15877
16	4.712	17.67	0.5275	3.2	8.25	3.55	1.23088

38.06°, 55.06°, 65.59° and 69.01° with (1 1 1), (2 0 0), (2 2 0), (3 1 1) and (2 2 2) planes of Cubic structure (JCPDS card no. 78-0653). Moreover, the peak intensity of CdO is increased with increasing the Cu intermetallic layer thickness. However, no peaks are observed corresponding to the Cu metallic interlayer. This can be qualified to the effect of CdO upper layer, which acts as a screen to prevent the detection of Cu by the instrument. Moreover, the diffusion of Cu into CdO layer is considered as another contributing factor [12, 13]. The preferential crystallite orientations in the CdO/Cu/CdO multilayer thin films can be exposed based on the texture coefficient ( $T_c$ ) using the following equation [14]:

$$T_c(hkl) = \frac{I(hkl)/I_0(hkl)}{N^{-1} \sum I(hkl)/I_0(hkl)}, \quad (1)$$

where  $T_c(hkl)$  is the texture coefficient,  $I(hkl)$  are the XRD intensities measured for CdO/Cu/CdO multilayer thin films,  $I_0$  is the standard intensity of CdO obtained from the JCPDS reference card and  $N$  is the number of considered diffraction peaks. According to  $T_c(hkl)$  values, when  $0 < T_c(hkl) < 1$  this refer to deficiency of grains oriented in a particular  $(hkl)$  direction. Though, if  $T_c(hkl) > 1$  this reflected that the abundance of grains is higher in that particular  $(hkl)$  direction and consequently the  $(hkl)$  plane is considered as the preferential orientation. The present calculations of  $T_c(hkl)$  revealed preferential orientations along (2 0 0) direction and the  $T_c(200)$  values are greater than the unity. Table 1 displays that the value of texture coefficient  $T_c(200)$  increased as the Cu intermetallic layer thickness increased. The increased in metallic interlayer thickness might prompted the growth in the orientation toward (2 0 0) plane direction.

Different micro-structural parameters that control the properties of CdO/Cu/CdO multilayer thin films and regulate their applications in microelectronics and optoelectronics are estimated and presented in Table 1. The lattice parameter “ $a$ ” is calculated based on inter planar spacing ( $d$ ). Bragg’s law ( $n\lambda = 2d \sin \theta$ ) was employed to determine the inter planar spacing “ $d$ ” then the parameter “ $a$ ” was calculated using the following relationship:

$$\frac{1}{d^2} = \frac{(h^2 + k^2 + l^2)}{a^2}, \quad (2)$$

where  $h$ ,  $k$ , and  $l$  are the Miller indices for the predominant orientation. The small difference observed in Table 1 between the standard (4.694 Å) and measured lattice parameter values can be recognized to the generation of defects during the deposition process. The crystallite size is calculated from Scherrer’s relationship [15]:

$$D = \frac{0.9 \lambda}{\beta \cos \theta}, \quad (3)$$

where  $D$  is the crystallite size, 0.9 is the shape factor,  $\beta$  is the FWHM,  $\theta$  is the diffracted angle, and  $\lambda$  is the wavelength of the incident X-rays. The average crystallite size for CdO single layer (CdO with thickness of 180 nm) recorded a value of 12.03 nm and it increased with increasing the Cu intermetallic layer thickness to reach a value of 17.67 nm for CdO/Cu (16 nm)/CdO multilayer thin film. As the metallic interlayer Cu thickness increased, the kinetic energy and mobility of ad-atoms increased to enhance the migration to the substrate’s surface and to provide the thermal energy required for crystallization [16]. Moreover, the individual smaller crystallites coalesced together to form larger crystallites with reduced grain boundaries and subsequently improved the crystallinity for the top CdO layers. From the micro-structural parameters calculations, it is apparent that the Bragg’s positions of the diffraction planes slightly shifted to higher angle and it was summarized in Table 1. The observed Bragg’s position shift is ascribed to compressive stress resulting in the interface between multilayers, which lead to peaks shift to high angles [17].

The micro-strain ( $\epsilon$ ), dislocation density ( $\delta$ ), and number of crystallites per unit area ( $N$ ) for CdO/Cu/CdO multilayer thin films are calculated using the following relationships [18]:

$$\epsilon = \frac{\beta \cot \theta}{4}, \quad (4)$$

$$\delta = \frac{1}{D^2}, \quad (5)$$

$$N = \frac{d}{D^3} \quad (6)$$

where  $d$  is the film thickness of the deposited CdO/Cu/CdO multilayers. Figure 2 displays the variations in the

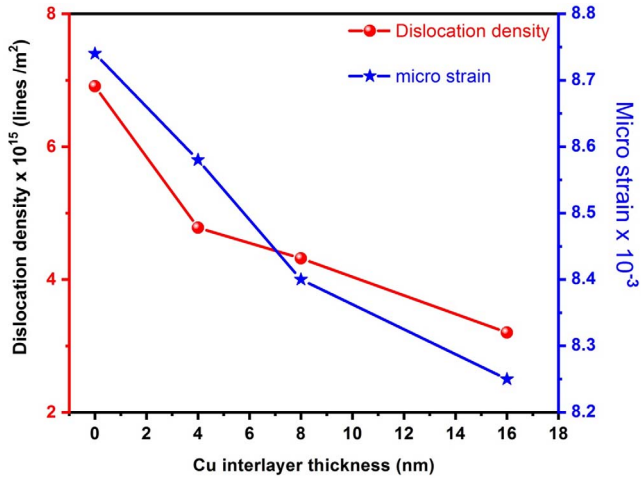


**Figure 2.** The micro-strain ( $\epsilon$ ) and dislocation density ( $\delta$ ) of CdO/Cu/CdO multilayer films with different Cu metallic interlayer thickness.

dislocation density and micro-strain for the multilayers with different Cu intermetallic layer thickness. The dislocation density decreased from  $6.91 \times 10^{15}$  to  $3.20 \times 10^{15}$  lines  $m^{-2}$  and the micro-strain decreased from  $8.74 \times 10^{-3}$  to  $8.25 \times 10^{-3}$  for CdO single layer and CdO/Cu (16 nm)/CdO multilayer film, respectively. The dislocation density and micro-strain are inversely proportional to the crystallite size. The lower value of dislocation density reflected higher crystallinity levels for the multilayer films, which is confirmed by XRD patterns [19]. As the crystallite size increased, the dislocation density decreased owed to the reduced concentration of lattice imperfections [20]. The number of crystallites per unit area ( $N$ ) is decreased as the crystallite size increased (see Table 1) which is attributed to the combination of adjacent small grains to form larger grains [21].

### 3.2 Optical properties of CdO/Cu/CdO multilayers films

Figures 3a and 3b illustrate the optical transmittance and reflectance spectra for CdO/Cu/CdO multilayer films, respectively. It can be discovered from Figure 3a that the CdO single-layer film has high optical average transmittance around 80% over the spectral range (300–2500 nm). Inclusion the Cu intermetallic layer between CdO top and bottom layers resulted in reducing the transmittance over the range of wavelength. Moreover, the increase in the Cu intermetallic layer thickness resulted in a notable reduction in the transmittance in the NIR spectrum range. The reduction in transmittance is qualified to the scattering by metallic surface and free electrons [22]. Moreover, the optical absorption by surface plasmon polaritons generated at the Cu/CdO interface is considered as supplementary relevant factor [13]. Similar results were demonstrated by Sahu and Huang [23] and Raaif and Mohamed [24]. Figure 3b illustrates that the reflectance of CdO/Cu/CdO multilayer films is increased with increasing the Cu intermetallic layer thickness owed to the scattering by the metallic Cu surface

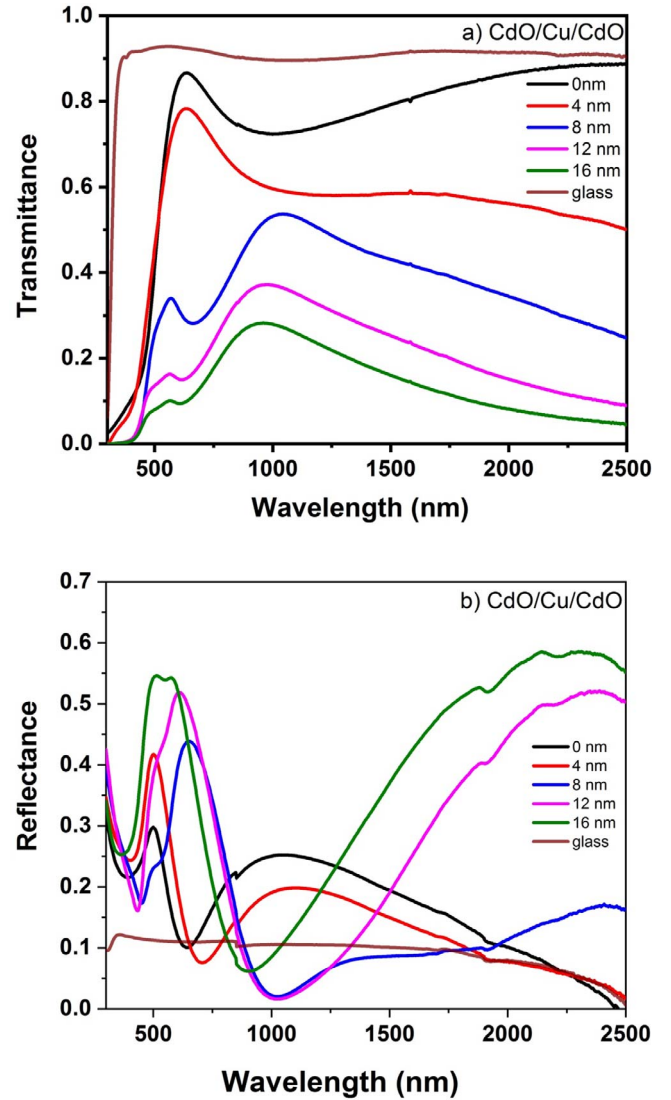


**Figure 3.** (a) Optical transmittance ( $T$ ) and (b) reflectance ( $R$ ) spectra of multilayer films with different Cu metallic interlayer thickness.

and free electrons. Supplementary, the increase in the roughness at the interface between top and bottom CdO layers can enhance the light scattering and reflectivity [24].

The refractive index ( $n$ ) and extinction coefficient ( $k$ ) of CdO/Cu/CdO multilayer films can be attained from the following equation [25]:

$$n = \left[ \left( \frac{4R}{(R-1)^2} - k^2 \right)^{\frac{1}{2}} - \frac{R+1}{R-1} \right]. \quad (7)$$

Using the film thickness  $d$ , the values of the optical absorption coefficient,  $\alpha$  can be estimated from the measurements of  $T(\lambda)$  and  $R(\lambda)$  using the relation

$$\alpha = \frac{1}{d} \ln \frac{(1-R^2)}{T}. \quad (8)$$

After that  $k$  can be calculated according to

$$k = \frac{\alpha\lambda}{4\pi}. \quad (9)$$

Figures 4a and 4b signified the spectral variation of  $n$  and  $k$  for CdO/Cu/CdO multilayer films as a function of wavelength for different Cu intermetallic layer thickness. It is witnessed from Figure 4a that the  $n$  value of single CdO layer and CdO/Cu/CdO multilayer films followed anomalous dispersion up to nearly 700 nm after that it followed normal dispersion up to nearly 900 nm. In the NIR region, the CdO single layer, CdO/Cu (4 nm)/CdO and CdO/Cu (8 nm)/CdO (low Cu metallic thickness) followed normal dispersion. However, the CdO/Cu (12 nm)/CdO and CdO/Cu (16 nm)/CdO (high Cu metallic thickness) followed anomalous dispersion in the NIR region. The structure and morphology of Cu intermetallic layer affected the disparity in the refractive index of the multilayers, which converted from isolated islands at low Cu thickness to an incessant structure at high thickness of Cu. The variation of the extinction coefficient of CdO/Cu/CdO multilayer films as a function of wavelength is presented in Figure 4b. It is observed that the  $k$  values increased as the wavelength increased for CdO single layer and CdO/Cu/CdO multilayers. Moreover, the  $k$  value is increased as the Cu intermetallic layer thickness increased which is recognized to the absorption by free electrons and metallic surface and the effect of surface plasmon generated at the CdO/Cu interface [12].

To determine the optical energy band gap  $E_g$  of CdO/Cu/CdO multilayer thin films, the following relationship is employed [26]:

$$\alpha h\nu = A(h\nu - E_g)^n, \quad (10)$$

where,  $A$  is the characteristic constant, which is independent of the photon energy for the transition,  $h$  is Planck's constant,  $\nu$  is the frequency of the incident photon and the exponent term  $n$  depends on the type of transition. For crystalline semiconductors, " $n$ " has different values of 1/2, 2, 3/2, and 3, which correspond to allowed direct, allowed indirect, forbidden direct and forbidden indirect transitions respectively. Figure 5 represents the relationship between  $(\alpha h\nu)^2$  and  $h\nu$  for CdO/Cu/CdO multilayers. The value of  $E_g$  is attained by extrapolating the linear portion to the photon energy axis in that figure. The assessed values of  $E_g$  for CdO/Cu/CdO multilayer films recorded lower values compared with single CdO layer that recorded 2.68 eV. The  $E_g$  is decreased from 2.65 to 2.48 eV as the Cu intermetallic layer decreased from 4 to 16 nm. The  $E_g$  value for CdO single layer is lower than the reported value (3.50 eV) by Thambidurai et al. [27] for CdO nanocrystalline thin films prepared by sol-gel spin coating. Zhang [28] and Yu et al. [29] demonstrated the behavior of decreasing the  $E_g$  as increasing the Cu metallic interlayer thickness for ZnO/Ag/ZnO and SnO<sub>2</sub>/Cu/SnO<sub>2</sub> multilayers respectively. The decrease in the band gap is related to the increase in free carrier concentrations resulting from inserting Cu intermetallic layer between the two metal oxide layers [30]. The decrease in lattice strain and dislocation density (which are achieved in the present work) are considered as other contributing

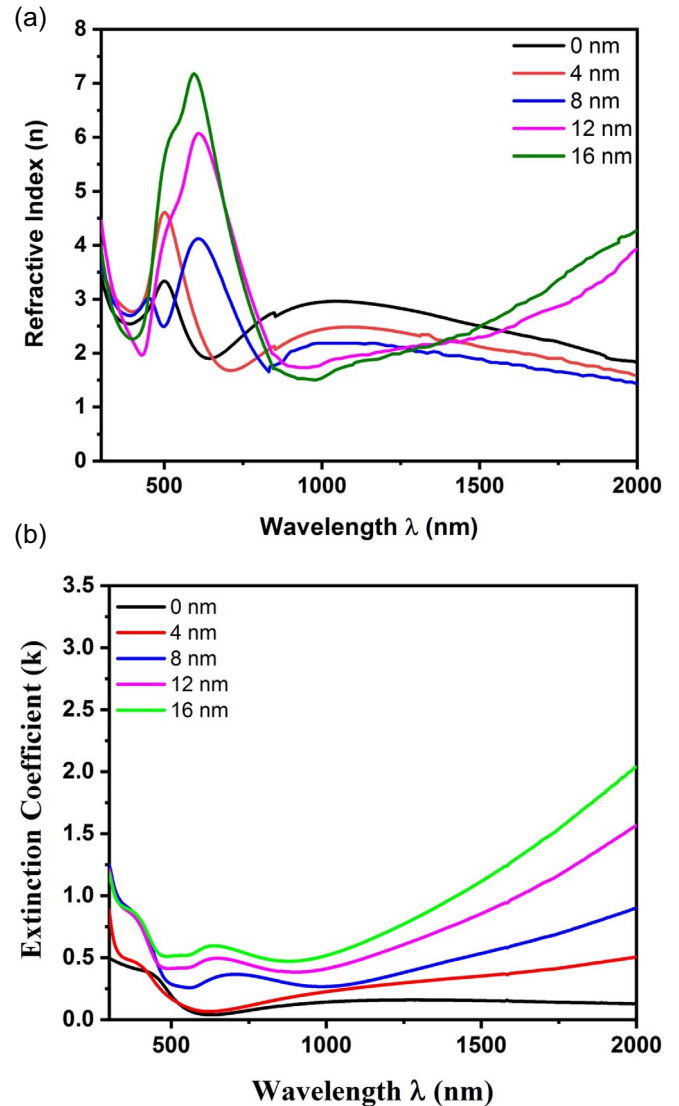


**Figure 4.** (a) Refractive index ( $n$ ) and (b) extinction coefficient of CdO/Cu/CdO multilayer films with different Cu metallic interlayer thickness.

factors that controlling the decrease in the optical band gap [31]. Further, the decrease of  $E_g$  with increasing Cu metallic layer thickness is due to the difference in work functions between two layers of CdO and Cu interlayer, which is responsible for spontaneous transferring of interfacial charge in these multilayers [32]. The electrons transfer from Cu layer into CdO layer at Cu/CdO interface, creating an accumulation of electrons in the metal oxide layer. The increase in carrier concentration upon inserting the Cu intermetallic layer in between CdO top and bottom layers can be assumed by taking into consideration the many body interactions model [16, 33, 34]. A schematic for the energy band diagram of Cu and CdO before and after their contact is presented in Figures 6a and 6b. When two layers (metal and metal oxide) got into contact and as the work function of Cu = 4.5 eV is lower than that of CdO = 5.38 eV, a diffusion of free carriers

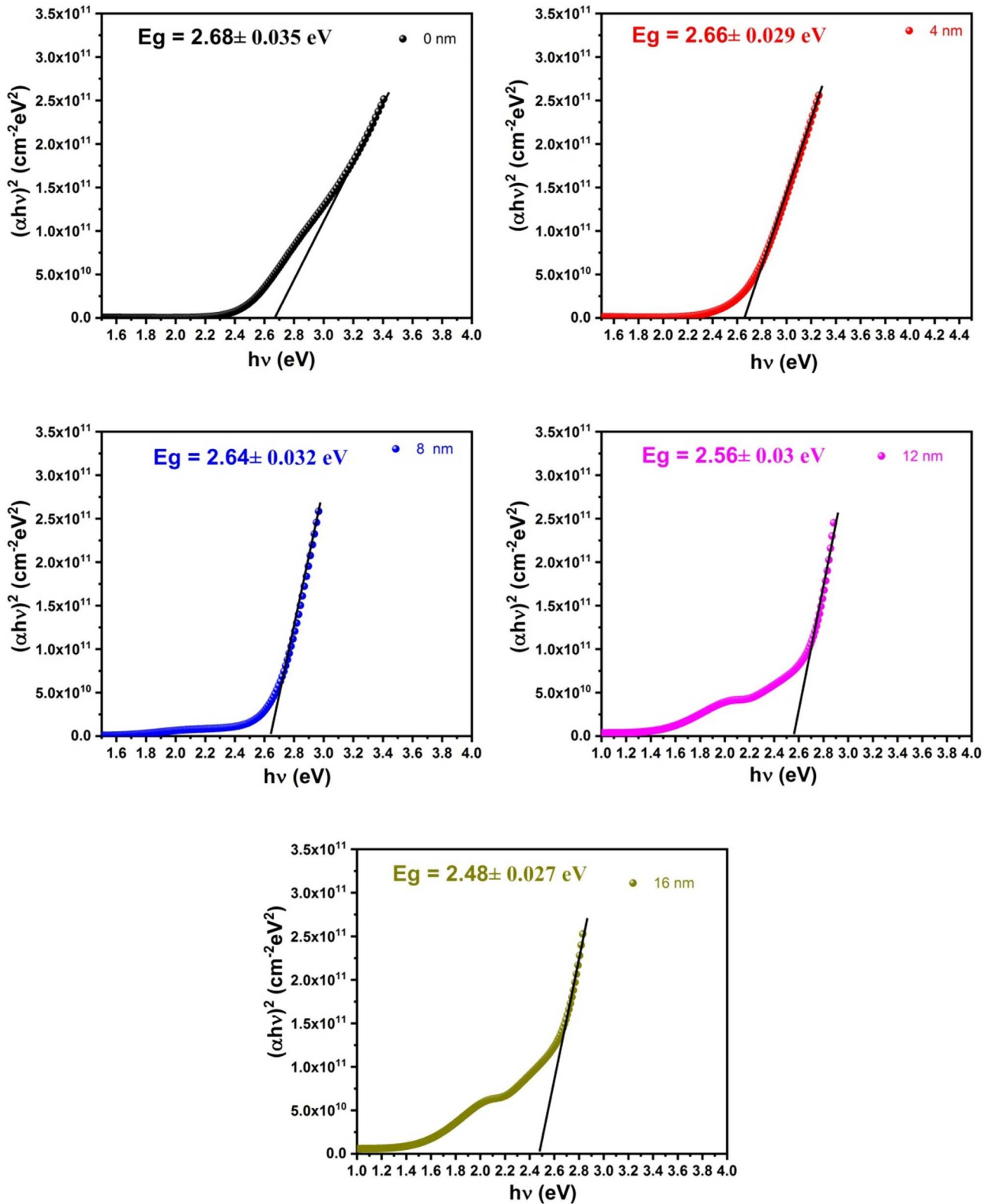


**Figure 5.** Plots of  $(\alpha hv)^2$  against  $(h\nu)$  for CdO/Cu/CdO multilayer films at different Cu metallic interlayer thickness.

(electrons) from Cu intermetallic layer to CdO layer is taking place and the Fermi levels are align at equilibrium. This resulted in an accumulation-type connection

between Cu and CdO owed to band bending at the contact. Consequently, there is no barrier for charges to transfer between the Cu and CdO layers. Subsequently,

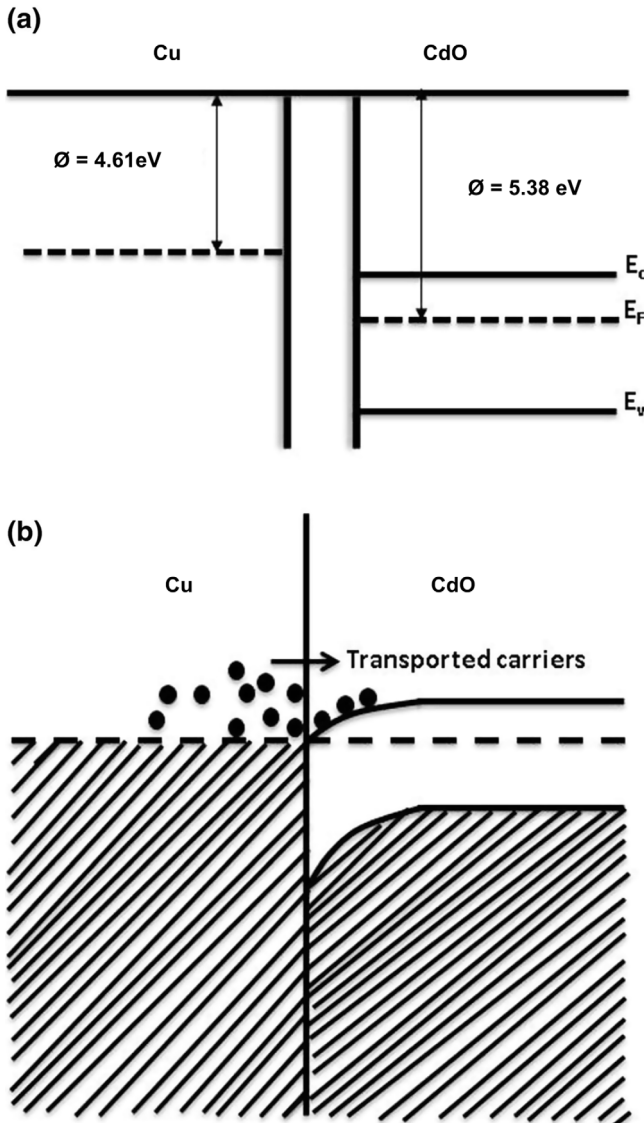


**Figure 6.** The schematic energy band structures for Cu and CdO (a) prior contact and (b) after contact.

the electron concentrations for the multilayer system is increased. The defused electrons from Cu intermetallic layer accumulated in CdO conduction band. On the other hand, some of Cu atoms in the adjacent layer can be ionized and become positively charged. The negative electrons in the conduction band attracted the positively charged Cu ions. Thus, the narrowed band gap can happen where the conduction band minimum of CdO shifts to the valence band maximum owing to the many body interactions. The increase in carrier concentration of the multilayer films with increasing Cu intermetallic layer thickness (Table 2) resulted in increasing the impurity or/and defect states such as oxygen vacancies and substitutional dopants in the stacked layer films. It should be stated that, the reduction in the  $E_g$  of the CdO/Cu/CdO multilayer films with increasing the Cu metallic interlayer thickness is more appropriate in the photo catalysts and chemical sensing devices.

The Urbach energy  $E_U$  is defined as the band tail width of the localized states in the optical energy gap and is given by exponential equations:

$$\alpha = \alpha_0 \exp\left(\frac{hw}{E_u}\right). \quad (11)$$

The Urbach energy was determined from the plot of  $\ln(\alpha)$  as a function of photon energy as seen in Figure 7. The estimated values of  $E_u$  increased from 338 to 689 meV as the Cu intermetallic layer thickness increased from 0 to 16 nm as presented in Table 2. The variation in the estimated values of  $E_u$  indicated that the Cu metallic interlayer thickness has a noteworthy impact in the band gap tailing.

### 3.3 Electrical properties of CdO/Cu/CdO multilayers films

The relation between resistivity, mobility and carrier concentration is given by the following formula [35]

$$\rho = \frac{1}{n e \mu}, \quad (12)$$

where  $\rho$ ,  $e$ ,  $\mu$ , and  $n$  are electrical resistivity, electronic charge, carrier mobility and carrier concentration, respectively. Details about the calculations of the presented electrical parameters can be found elsewhere [25]. Figure 8 represents the resistivity, mobility and carrier concentration of CdO/Cu/CdO multilayers films with variation in Cu intermetallic layer thickness. Moreover, the conductivity and sheet resistance are presented in Table 2. It can be observed from Figure 8 and Table 2 that the carrier concentration value increased as the Cu metallic interlayer thickness increased to reach a value of  $2.67 \times 10^{20} \text{ cm}^{-3}$  for CdO/Cu (16 nm)/CdO multilayer film, which represented the suitable carrier concentration value needed for TCO materials [36]. One can observe also that the single layer CdO has poor mobility value and it increased with increasing the Cu metallic interlayer thickness. On the other hand, the resistivity is decreased as the Cu thickness increased to reach a value of  $2.7 \times 10^{-4} \Omega \text{ cm}$  for CdO/Cu (16 nm)/CdO. A significant amount of current can pass through the copper layer leading to a decrease in the resistivity with increasing Cu intermetallic layer thickness. As increasing the Cu intermetallic layer, the mobility and carrier concentration increased which in turn a decrease in the resistivity is observed. Once the Cu and CdO are interfaced, the interfacial charge transfer will cause the variation of electrostatic potential distribution at the interface of CdO/Cu/CdO multilayers. Abundant electrons are introduced from Cu layer into CdO layer due to the Fermi levels align at equilibrium. Hence, the value of carrier concentration in the CdO/Cu/CdO multilayers overrides the single CdO layer. In addition, the increase in mobility with increasing the Cu intermetallic thickness may be attributed to the reduction in the interface scattering between the Cu and CdO layers [16].

A figure of merit is considered as a tool to evaluate the best combination of high transmittance and low resistance of the transparent conductor CdO/Cu/CdO

**Table 2.** The Urbach energy, and the electrical properties including the resistivity, carrier concentration, sheet resistance and mobility for CdO/Cu/CdO multilayer films with different Cu metallic interlayer thickness.

Cu thickness (nm)	Urbach energy $E_u$ (meV)	Carrier concentration ( $\times 10^{20} \text{ cm}^{-3}$ )	Mobility ( $\text{cm}^2 \text{ V}^{-1} \text{ s}^{-1}$ )	Resistivity ( $\times 10^{-4} \Omega \text{ cm}$ )	Conductivity ( $\Omega^{-1} \text{ cm}^{-1}$ )	Sheet resistance ( $\Omega/\text{sq}$ )	average transmittance ( $T_{av}$ )
0	338	2.09	1.65	180	0.555	1000	0.782
4	370	2.18	15.45	18.5	5.405	100	0.687
8	553	2.29	46.11	5.9	16.95	31.4	0.54
12	613	2.40	63.36	4.1	24.39	21.4	0.372
16	689	2.67	86.54	2.7	37.04	13.8	0.28

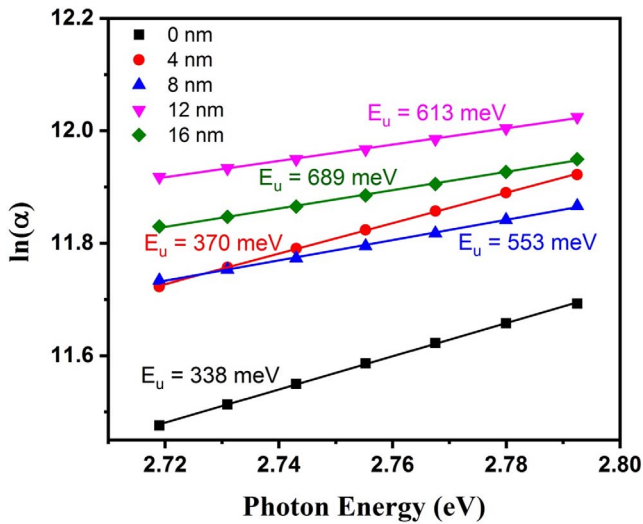


**Figure 7.** Plots of  $\ln(\alpha)$  versus  $(h\nu)$  for CdO/Cu/CdO multilayer films for different Cu metallic interlayer thickness.

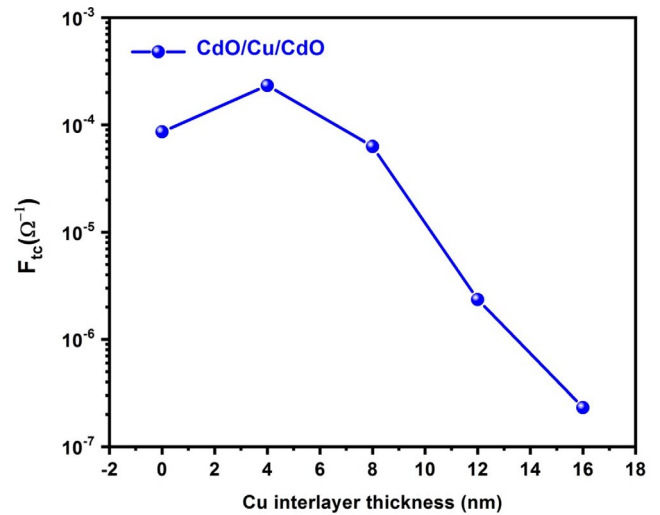


**Figure 9.** The variation of  $F_{TC}$  with Cu intermetallic layer thickness for CdO/Cu/CdO multilayer thin films.

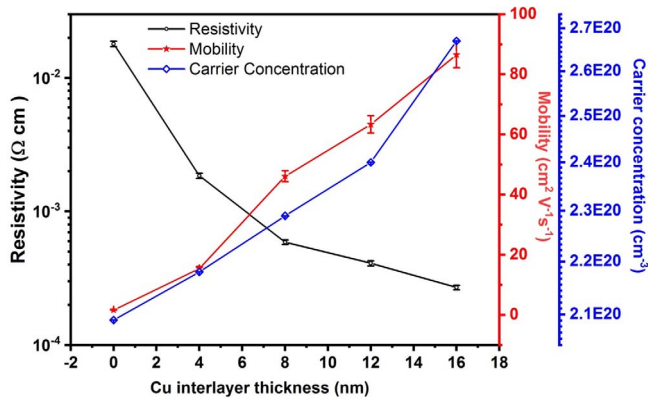


**Figure 8.** The resistivity, mobility and carrier concentration of CdO/Cu/CdO multilayers films with variation in Cu interlayer thickness.

multilayer thin films, which can be calculated from Haacke's equation [37]:

$$F_{TC} = \frac{T_{av}^{10}}{R_s} \quad (13)$$

where  $T_{av}$  is the average transmittance in the high transmittance range and  $R_s$  is the sheet resistance. Figure 9 displays the variation of  $F_{TC}$  with Cu intermetallic layer thickness for CdO/Cu/CdO. One can witness that the CdO/Cu (4 nm)/CdO multilayer has the best  $F_{TC}$  ( $2.3 \times 10^{-4} \Omega^{-1}$ ). This value is close to the value about  $2.8 \times 10^{-4} \Omega^{-1}$  for the ZnO (30 nm)/Cu (21 nm)/ZnO (30 nm) hybrids, which is used also as a transparent conductive electrodes for optoelectronic devices [28].

### 3.4 Wettability and contact angle of CdO/Cu/CdO multilayers films

Figure 10 displays the variation of contact angle before and after sunlight illumination at 1-hour duration for multilayers CdO/Cu/CdO films with different Cu interlayer thickness. Before illumination, the measured contact angles are  $84^\circ$ ,  $85^\circ$ ,  $86^\circ$ ,  $91^\circ$ , and  $80^\circ$  for CdO/Cu/CdO multilayers with Cu metallic interlayer thickness of 0, 4, 8, 12 and 16 nm, respectively. After sunlight illumination, the contact angle decreased sharply for CdO/Cu/CdO multilayers thin films and the multilayers films transformed to hydrophilic nature. The contact angle recorded lowest value equal to  $24^\circ$  for CdO/Cu (8 nm)/CdO and CdO/Cu



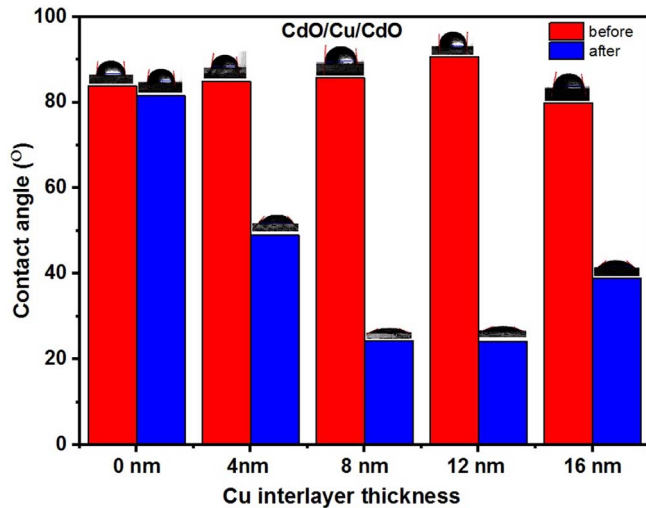


**Figure 10.** the variation of contact angle before and after sunlight illumination at one-hour duration for CdO/Cu/CdO multilayer films with different Cu interlayer thickness.

(12 nm)/CdO. In the presented results, the surface wettability before illumination for CdO thin film agrees well with Chug et al. [38]. Chug et al. represented hydrophobic surface wettability for crystalline CdO thin film prepared by chemical deposition. Sankarasubramanian et al. [39] prepared CdO thin film by spray pyrolysis method with different concentration of cadmium acetate and demonstrated an increase in water contact angle from 93° to 133° with increasing the precursor concentrations from 0.025 M to 0.1 M. Rico et al. [40] demonstrated that the irradiation with ultraviolet light for ITO thin film changed the water contact angle from 110° to 10° after irradiation for one hour. The decrease in water contact angle for CdO/Cu/CdO multilayer films after illumination by sunlight is inter-related to the production of oxygen vacancy on the surface; these vacancies enhanced the adsorption of water molecules [41]. On the other hand, the illumination by sunlight may be increased the mobility of the free carrier in the Cu interlayer which in turn enhanced the surface energy and decreased the contact angle.

## Conclusions

Multilayer films of CdO/Cu/CdO structure were arranged by DC plasma pulsed magnetron sputtering. Optimizing the growth conditions of a Cu intermetallic layer can result in desired electrical and optical properties. The transmission for CdO/Cu/CdO multilayer films decreased in the visible range with increasing the Cu intermetallic layer thickness. Besides, the effect of free electrons and surface plasmon provided by the metallic Cu interlayer resulted in decreasing the transmission in the NIR region. The estimated band gap reduced from 2.66 eV to 2.48 eV as the Cu interlayer thickness increased from 4 to 16 nm and the resistivity is decreased to reach a value of  $2.7 \times 10^{-4} \Omega \text{ cm}$  for CdO/Cu (16 nm)/CdO multilayer film. Further, CdO/Cu

(4 nm)/CdO multilayer film recorded the best figure of merit ( $2.3 \times 10^{-4} \Omega^{-1}$ ) which can be potentially used as electrode. The results of exposure to sunlight illumination demonstrated a decrease in water contact angle for CdO/Cu (8 nm)/CdO and CdO/Cu (12 nm)/CdO which are appropriated for self-cleaning surfaces and may be used as solar panel coatings.

## Conflict of interest

The authors declare no conflict of interest.

*Acknowledgments.* The author (A.A. Abd El-Moula) extend their appreciations to the Deanship of Scientific Research of Jouf University for funding this work through research grant No. (DSR 2020-02-464).

## References

- 1 Aissa B., Abdallah A.A., Zakaria Y., Kivambe M.M., Samara A., Shetty A.R., Cattin J., Haschke J., Boccard M., Ballif C. (2019) Impact of the oxygen content on the optoelectronic properties of the indiumtin-oxide based transparent electrodes for silicon heterojunction solar cells, *AIP Conf. Proc.* **2147**, 030001. <https://doi.org/10.1063/1.5123827>.
- 2 Yoshikawa K., Kawasaki H., Yoshida W., Irie T., Konishi K., Nakano K., Uto T., Adachi D., Kanematsu M., Uzu H., Yamamoto K. (2017) Silicon heterojunction solar cell with interdigitated back contacts for a photoconversion efficiency over 26%, *Nature Energ.* **2**, 17032. <https://doi.org/10.1038/nenergy.2017.32>.
- 3 Fujiwara H., Kondo M. (2005) Effects of carrier concentration on the dielectric function of ZnO: Ga and In<sub>2</sub>O<sub>3</sub>: Sn studied by spectroscopic ellipsometry: Analysis of free-carrier and band-edge absorption, *Phys. Rev. B* **71**, 075109. <https://doi.org/10.1103/PhysRevB.71.075109>.
- 4 Farhan M.S., Zalnezhad E., Bushroa A.R., Sarhan A.A.D. (2013) Electrical and optical properties of indium-tin oxide (ITO) films by ion-assisted deposition (IAD) at room temperature, *Int. J. Precis. Eng. Manuf.* **14**, 8, 1465–1469. <https://doi.org/10.1007/s12541-013-0197-5>.
- 5 Sakthivel P., Asaithambi S., Karuppaiah M., Sheikfareed S., Yuvakkumar R., Ravi G. (2019) Different rare earth (Sm, La, Nd) doped magnetron sputtered CdO thin films for optoelectronic applications, *J. Mater. Sci.: Mater. Electron.* **30**, 9999–10012. <https://doi.org/10.1007/s10854-019-01342-9>.
- 6 Grundmann M. (2015) Karl Bädcker (1877–1914) and the discovery of transparent conductive materials, *Phys. Status Solidi.* **212**, 1409–1426. <https://doi.org/10.1002/pssa.201431921>.
- 7 Mohamed S.H., Zhao H., Romanus H., El-Hossary F.M., Abo El-Kassem M., Awad M.A., Rabia M., Lei Y. (2020) Optical, water splitting and wettability of titanium nitride/titanium oxynitride bilayer films for hydrogen generation and solar cells applications, *Mater. Sci. Semicond. Process.* **105**, 104704. <https://doi.org/10.1016/j.mssp.2019.104704>.
- 8 Mozumder M.S., Mourad A.I., Pervez H., Surkatti R. (2019) Recent developments in multifunctional coatings for solar panel applications: A review, *Sol. Energy Mater. Sol. Cells* **189**, 75–102. <https://doi.org/10.1016/j.solmat.2018.09.015>.

- 9 Pan Z., Cao S., Li J., Du Z., Cheng F. (2019) Anti-fouling TiO<sub>2</sub> nanowires membrane for oil/water separation: Synergetic effects of wettability and pore size, *J. Membr. Sci.* **572**, 596. <https://doi.org/10.1016/j.memsci.2018.11.056>.
- 10 El-Hossary F.M., Abd El-Rahman A.M., Raaif M., Shuxin Q., Zhao J., Manfred F.M., Abo El-kassem M. (2018) Effect of DC-pulsed magnetron sputtering power on structural, tribological and biocompatibility of Ti-Zr-N thin film, *Appl. Phys. A* **124**, 42. <https://doi.org/10.1007/s00339-017-1462-8>.
- 11 El-Hossary F.M., Mohamed S.H., Noureldein E.A., Abo El-Kassem M. (2021) ZnO thin films prepared by RF plasma chemical vapour transport for self-cleaning and transparent conducting coatings, *Bull. Mater. Sci.* **44**, 82. <https://doi.org/10.1007/s12034-021-02378-6>.
- 12 Abd El-Moula A.A., El-Hossary F.M., Raaif M., Thabet A., Abo El-Kassem M. (2021) Effect of Cu metallic interlayer thickness on optoelectronic properties of TiO<sub>2</sub>-based multilayers deposited by DC pulsed magnetron sputtering, *J. Electron. Mater.* **50**, 5, 2699–2709. <https://doi.org/10.1007/s11664-021-08781-3>.
- 13 Abo El-Kassem M., El-Hossary F.M., Raaif M., Aroua W., Thabet A., Abd El-Moula A.A. (2021) Optoelectronic properties and surface plasmon polaritons of CdO/Ag/CdO multilayer films deposited by DC pulsed magnetron sputtering, *J. Electron. Mater.* **50**, 4933–4944. <https://doi.org/10.1007/s11664-021-09025-0>.
- 14 Barrett C.S., Massalski T.B. (1980) *Structures of metals*, Vol. **204**, Pergamon, Oxford.
- 15 Murugan R., Vijayaprasath G., Ravi G. (2015) The influence of substrate temperature on the optical and micro structural properties of cerium oxide thin films deposited by RF sputtering, *Superlattices Microstruct.* **85**, 321–330. <https://doi.org/10.1016/j.spmi.2015.05.041>.
- 16 Han H., Theodore N.D., Alford T.L. (2008) Improved conductivity and mechanism of carrier transport in zinc oxide with embedded silver layer, *J. Appl. Phys.* **103**, 013708. <https://doi.org/10.1063/1.2829788>.
- 17 Ni J., Li J., Jian J., He J., Chen H., Leng X., Liu X. (2021) Recent studies on the fabrication of multilayer films by magnetron sputtering and their irradiation behaviors, *Coatings* **11**, 12, 1468. <https://doi.org/10.3390/coatings11121468>.
- 18 Shrividhya T., Mahalingam T., Ravi G. (2015) Physical property exploration of highly oriented V<sub>2</sub>O<sub>5</sub> thin films prepared by electron beam evaporation, *New J. Chem.* **39**, 9471–9479. <https://doi.org/10.1039/C5NJ01582K>.
- 19 Sahare S., Choubey R.K., Jadhav G., Bhave T.M., Mukherjee S., Kumar S. (2017) A comparative investigation of optical and structural properties of Cu-doped CdO-derived nanostructures, *J. Supercond. Nov. Magn.* **30**, 1439–1446. <https://doi.org/10.1007/s10948-016-3943-y>.
- 20 Sakthivel P., Murugan R., Asaithambi S., Karuppaiyah M., Vijayaprasath G., Rajendran S., Hayakawa Y., Ravi G. (2018) Radiofrequency power induced changes of structural, morphological, optical and electrical properties of sputtered cadmium oxide thin films, *Thin Solid Films* **654**, 85–92. <https://doi.org/10.1016/j.tsf.2018.04.004>.
- 21 Sakthivel P., Murugan R., Asaithambi S., Karuppaiyah M., Rajendran S., Ravi G. (2019) Radio frequency magnetron sputtered CdO thin films for optoelectronic applications, *J. Phys. Chem. Solids* **126**, 1–10. <https://doi.org/10.1016/j.jpcs.2018.10.031>.
- 22 Anitha M., Saravanakumar K., Anitha N., Kulandaisamy I., Amalraj L. (2019) Influence of annealing temperature on physical properties of Sn-doped CdO thin films by nebulized spray pyrolysis technique, *Mater. Sci. Eng. B* **243**, 54–64. <https://doi.org/10.1016/j.mseb.2019.03.018>.
- 23 Sahu D.R., Huang J.L. (2006) Dependence of film thickness on the electrical and optical properties of ZnO–Cu–ZnO multilayers, *Appl. Surf. Sci.* **253**, 915–918. <https://doi.org/10.1016/j.apsusc.2006.01.035>.
- 24 Raaif M., Mohamed S.H. (2017) The effect of Cu on the properties of CdO/Cu/CdO multilayer films for transparent conductive electrode applications, *Appl. Phys. A* **123**, 441. <https://doi.org/10.1007/s00339-017-1050-y>.
- 25 Abeles F. (1972) *Optical properties of solids*, North Holland, Amsterdam.
- 26 Tauc J. (1974) in *Amorphous and liquid semiconductors*, J. Tauc (ed), Plenum Press, London and New York.
- 27 Thambidurai M., Muthukumarasamy N., Ranjitha A., Velauthapillai D. (2015) Structural and optical properties of Ga-doped CdO nanocrystalline thin films, *Superlattices Microstruct.* **86**, 559. <https://doi.org/10.1016/j.spmi.2015.08.020>.
- 28 Zhang Z. (2019) Effect of copper evolution on photoelectric properties of ZnO/Cu/ZnO hybrids, *App. Phys. A* **125**, 9, 584. <https://doi.org/10.1007/s00339-019-2889-x>.
- 29 Yu S., Li L., Xu D., Dong H., Jin Y. (2014) Characterization of SnO<sub>2</sub>/Cu/SnO<sub>2</sub> multilayers for high performance transparent conducting electrodes, *Thin Solid Films* **562**, 501. <https://doi.org/10.1016/j.tsf.2014.04.064>.
- 30 Raaif M., Abd El-Moula A.A., El-Hossary F.M., Aroua W., Abo El-Kassem M. (2022) Optoelectronic properties of ZrO<sub>2</sub>/Cu/ZrO<sub>2</sub> multilayers prepared by DC pulsed magnetron sputtering for electrode and nano-filter applications, *ECS J. Solid State Sci. Technol.* **11**, 085011. <https://doi.org/10.1149/2162-8777/ac8a74>.
- 31 Segura A., Sánchez-Royo J.F., García-Domene B., Almonacid G. (2011) Current underestimation of the optical gap and Burstein-Moss shift in CdO thin films: A consequence of extended misuse of  $\alpha^2$ -versus-hv plots, *Appl. Phys. Lett.* **99**, 151907. <https://doi.org/10.1063/1.3651338>.
- 32 Gong L., Lu J.G., Ye Z.Z. (2011) Conductive Ga doped ZnO/Cu/ Ga doped ZnO thin films prepared by magnetron sputtering at room temperature for flexible electronics, *Thin Solid Films* **519**, 3870–3874. <https://doi.org/10.1016/j.tsf.2011.01.396>.
- 33 Awad M.A., Raaif M. (2018) Optical and electrical performance of transparent conductive TiO<sub>2</sub>/Cu/TiO<sub>2</sub> multilayers prepared by magnetron sputtering, *J. Mater. Sci.: Mater. Electron.* **29**, 2815–2824. <https://doi.org/10.1007/s10854-017-8210-x>.
- 34 Indluru A., Alford T.L. (2009) Effect of Ag thickness on electrical transport and optical properties of indium tin oxide–Ag–indium tin oxide multilayers, *J. Appl. Phys.* **105**, 123528. <https://doi.org/10.1063/1.3153977>.
- 35 Calnan S., Tiwari A.N. (2010) High mobility transparent conducting oxides for thin film solar cells, *Thin Solid Films*. **518**, 1839–1849. <https://doi.org/10.1016/j.tsf.2009.09.044>.
- 36 Minami Tadatsugu. (2013) Transparent conductive oxides for transparent electrode applications, *Semicond. Semimet.* **88**, 159–200. <https://doi.org/10.1016/B978-0-12-396489-2.00005-9>.
- 37 Haacke G. (1976) New figure of merit for transparent conductors, *J. Appl. Phys.* **47**, 4086. <https://doi.org/10.1063/1.323240>.
- 38 Chug P.N., Padalkar P.R., Jamadade V.S., Lokhande C.D. (2014–2015) Chemically deposited polycrystalline CdO thin films, *Journal of Shivaji University (Science & Technology)* **41**, 2, 1.

- 39 Sankarasubramanian K., Soundarrajan P., Sethuraman K., Ramesh Babu R., Ramamurthi K. (2014) Structural, optical and electrical properties of transparent conducting hydrophobic cadmium oxide thin films prepared by spray pyrolysis technique, *Superlattices Microstruct.* **69**, 29–37. <https://doi.org/10.1016/j.spmi.2014.01.018>.
- 40 Rico V., López C., Borrás A., Espinós J.P., González-Elipé A.R. (2006) Effect of visible light on the water contact angles on illuminated oxide semiconductors other than TiO<sub>2</sub>, *Solar Energy Materials & Solar Cells* **90**, 2944–2949. <https://doi.org/10.1016/j.solmat.2006.05.005>.
- 41 Miyauchi M., Nakajima A., Watanabe T., Hashimoto K. (2002) Photocatalysis and photoinduced hydrophilicity of various metal oxide thin films, *Chem. Mater.* **14**, 2812–2816. <https://doi.org/10.1021/cm020076p>.